EARTHQUAKE OF 30 OCTOBER 2020 IN THE AEGEAN SEA: NUMERICAL SIMULATION OF THE GENERATION AND PROPAGATION OF TSUNAMI WAVES

Mazova R.Kh.[1,2], Kurkin A.A.[1], Giniyatullin A. R.[1], Tyuntyayev C.M.[3]

[1]*Nizhny Novgorod State Technical University n.a. R.E. Alekseev, 24, Minin str., 603950 Nizhny Novgorod, Russia. e-mail address: raissamazova@yandex.ru; aakurkin@gmail.com; adel.giniyatullin@gmail.com*
[2]*Moscow Institute of Physics and Technology (MIPT), Moscow Region, Russia*
[3]*Nizhny Novgorod , HARMAN, 8, Kovalikhinskaya st., 603006 Nizhny Novgorod, Russia., e-mail address: ser.tyuntyaev@gmail.com*

ABSTRACT

The paper considers the earthquake in Samos on October 30, 2020 and the subsequent tsunami. Based on the data on both intensity of the earthquake and localization of the epicenter of the earthquake and aftershocks, taking into account the tectonic setting for this region, where active tension and shear deformations coexist, two possible sources of the earthquake were considered. Virtual sources have been constructed along the fault zone north of Samos. Using the keyboard model of the earthquake, the optimal kinematic movements of the keyboard blocks in the earthquake source were found, which most adequately describe the generation of the tsunami source and the propagation of tsunami waves to the coastal zone. 3D histograms of the distribution of the maximum wave heights along the coast were constructed and compared with the available field data and data from other authors.

Keywords: tsunamigenic earthquakes, keyboard model, tsunami waves, numerical simulation.

1. INTRODUCTION

The Eastern Mediterranean Sea is one of the most seismically active areas, including the Aegean Sea and Western Anatolia. The cause for this activity is the movement of the Anatolian block towards the Aegean Sea. The expansion rate of the Earth's crust between Samos and Western Anatolia (the wider region of Izmir) is 7.4 mm/yr based on GNSS data simulations [1-6]. Seismic activity is mainly focused on normal faults, which are formed due to the active expansion of the West Anatolian plate in the southern and northern directions (white arrows in Fig.1). Active parts of the North Anatolian fault act as a source of strike-slip faults in the North Aegean Sea, which are located up to the island of Samos [11]. The earthquake on Samos on October 30, 2020 occurred in the region between the eastern islands of the Aegean Sea and Western Turkey, where there is an active tectonic regime (Fig.1) [1-6]. The available mechanisms of earthquake sources clearly confirm the coexistence of deformations along the coastal region of Western Anatolia and the Aegean Sea [5,6,11,38,40].
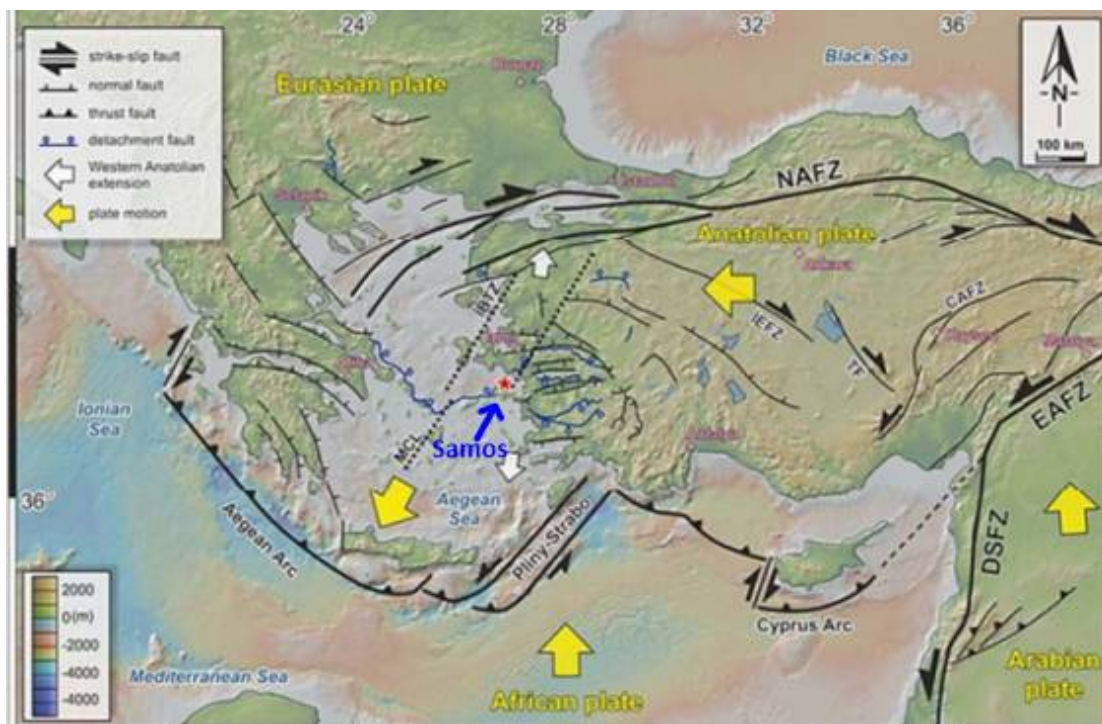

Fig. 1. Tectonic Map of Western Anatolia Region and the Aegean Sea [5, 6]. Yellow arrows indicate the motion of tectonic plates. The blue arrow points to the Samos Island. The red asterisk corresponds to the epicenter of the October 30, 2020 submarine earthquake.

The occurrence of large earthquakes in the 21st century and the associated tsunamis in the Mediterranean Sea is a great danger [39]. Turkey is crossed by large fault lines (see Fig.1), and is among the most earthquake-prone countries in the world [41-43]. For example, on August 17, 1999, off the coast of the Sea of Marmara in Turkey, there was an earthquake of magnitude $M = 7.5$. This earthquake caused great destruction, affecting even part of Istanbul. The tsunami that emerged after the earthquake (wave height 2.9 meters) hit the coastal areas of Turkey and led to their flooding [2,3].

It is well known that densely populated coastal areas in the Aegean Sea have been subject to several devastating tsunamis in the past (see, e.g., Altınok & Ersoy, 2000; Altınok et al., 2011; Ambraseys, 1962; Ambraseys & Synolakis, 2010; Dominey-Howes, 2002; Galanopoulos, 1960;

Kuran & Yalciner, 1993; Minoura et al., 2000; Papadopoulos & Chalkis, 1984; Papadopoulos et al., 2014; Soloviev et al., 1997; Tinti et al. 2001) [5,6]. The most famous tsunami in the region is the 1956 Amorgos event ($M \sim 7.8$), which caused waves up to 25 m high (Beisel et al. 2009; Okal et al. 2009; Papadopoulos & Pavlides, 1992; Papazachos, 1985; Yalciner et al. 1995) [5,6]. On October 30, 2020, a strong earthquake with a magnitude $M = 7.0$ occurred in the Aegean Sea, which was felt both in Greece and in Turkey [1,2, 21-23]. This earthquake epicenter was located north of the island of Samos in the area of the North Samos fault or the Kaistrios fault (Greece), with coordinates (37.88 N, 26.70 E) [5]. Initial estimates of magnitudes by various agencies ranged from 6.6 to 7.0 and the epicenter near (37.8919N; 26.8066E) [6,24]. The event with a magnitude of $M = 7.0$ slightly exceeds the maximum value expected for this subduction zone. Historical archives do not indicate an event of this magnitude on one or another local fault in the last 19 centuries (since 47 AD) [11-14]. Figure 2 shows a map of the water area with the epicenter of the earthquake and aftershocks, as well as the fault zone during the earthquake of October, 30, 2020 in the Aegean Sea [1-6].
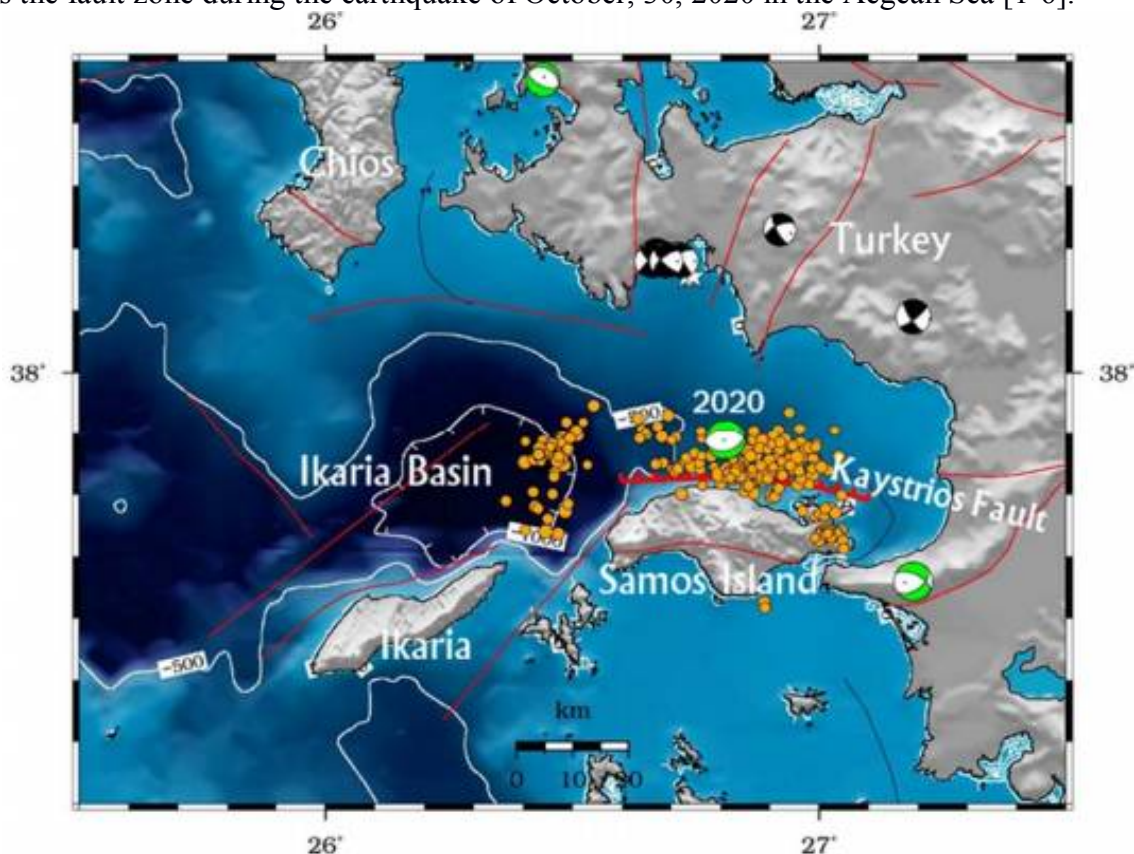

Fig. 2. Map of aftershocks and the epicenter of the earthquake on October 30, 2020. Samos, Greece. Bold red line north of Samos is the fault line [6]

As is known, aftershocks usually occur in the same fault or close to it at a distance of about twice the length of the fault zone, and the location of aftershock epicenters covers the zone of rupture of the main shock. It follows from the distribution of the aftershock sequence (Fig.2) that the fault occurred during the main shock $M = 7.0$, located off the northern coast of Samos Island. This fault in the region of Western Anatolia and the Aegean Sea can be identified as an oblique subduction zone [11].

Both countries experienced high tidal waves that led to flooding in parts of the Izmir coastline. The earthquake-triggered tsunami struck many nearby coastal areas. According to available materials, the water first receded from the coast, then soon the water returned, flooding low-lying coastal areas up to 1-2 meters high, including many coastal cities [5,6].

The tsunami generated by this earthquake was recorded in both Greece and Turkey [1]. The tsunami occurred as a sequence of sea level sink and surge [5]. The results of field studies following this event, carried out by a team of researchers along the 110 km coastline, demonstrated "… a significant tsunami impact. The maximum tsunami height in the area of pp. Kaleici in Sigacik was 2.3 m, " [5]. The results of this field study provide insight into the impact of near-field tsunamis on the coasts of the Aegean Sea.

In this work, based on both data on the intensity of the earthquake and the localization of the epicenter of the earthquake and aftershocks, taking into account the data on the subduction zone [1-6] (Table 1), two possible model sources of the earthquake were constructed.

Table 1. Parameters of the earthquake of October 30, 2020 in the Aegean Sea [6]

Earthquake Magnitude	7.0M
Depth	21 km
Lat/Lon	37.9175, 26.7901
Event Data	30 Oct 2020 11:51 UTC 30 Oct 2020 13:51 Local

The two-block and three-block earthquake sources located along the fault zone running to the north of the island of Samos are considered. Using keyboard model of the earthquake [27], which is briefly described in the next section, the optimal kinematic movements of the keyboard blocks in the earthquake source were found, which most adequately describe the generation of the tsunami source and the propagation of tsunami waves to the coastal zone.

2. ANALYSIS OF THE TSUNAMI SOURCE GENERATION MECHANISM

It is well known that the strongest earthquakes occur in fault zones, which are clearly visible on the bathymetric map (Fig.2), where the earthquake in question occurred. Since a strong earthquake as a result of the rapid movement of the seabed triggers a tsunami over its source zone, the vertical component of the dynamic displacement of rocks (schematically represented by the keyboard blocks) gives the displacement at the ocean surface, i.e. a tsunami source is formed [25]. The formation of a tsunami is influenced by the nature and dynamics of displacements in the zone of the earthquake source [26]. To compute the generation of tsunami waves, as a rule, seismic data are used, which make it possible to determine the orientation of the rupture in the source and the energy of the tsunami (see, for example, [44]).

a)   b)
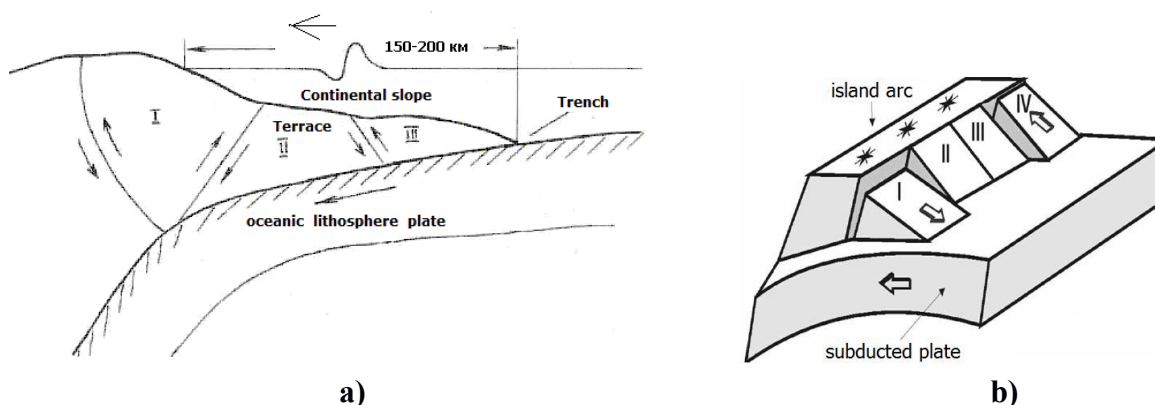
Fig. 3. a) Schematic representation of the frontal part of the island arc; b) Keyboard model of the blocks structure in the frontal part of the island arc [27].

Vol 40 No. 3, page 181 (2021)

4

In this paper, we consider the final fault with parameters obtained on the basis of the data given in [5]. The earthquake source is considered within the framework of a simplified keyboard model of the subduction zone [27]. Figure 3 shows a schematic representation of the block structure of the frontal part of the continental slope and the interaction of its main elements with the driven plate and with each other [27]. In Fig. 3a, one can see transverse faults - ruptures and movements in the source of tsunamigenic earthquakes. Figure 3b shows a model image of a subduction zone - a keyboard model of an earthquake source [27].

Since the question of the mechanism of the seismic source for an earthquake is still open [25], then setting the source mechanism from tectonic considerations, and using the Wells formula [33], based on the magnitude of the earthquake of a given event, we get an opportunity to calculate approximate data on the length of the rupture in the source and the width of the rupture plane. The vertical component of the wave surface displacement above the source of the earthquake is found via the Iida formula (see, for example, [26]). Thus, using formulas (1) and (2), the characteristics of the seismic source and the displacement of the water surface above the source of the earthquake were obtained (Table 2).

$$\lg L\,(km) = 0,59\,M - 2,44 \pm 0.16$$
$$\lg W\,(km) = 0,32\,M - 1,01 \pm 0.15 \qquad (1)$$

$$\lg(H,m) = 0,8M - 5,6 \pm 0.4 \qquad (2)$$

where M is the magnitude of the earthquake, L is the length of the rupture in the source (km), W is the width of the rupture plane (km), H is the maximum height of the vertical displacement of the water surface above the seismic source (m). Since the processes occurring in the seismic source during a strong earthquake (up thrust or fault) are ultimately recalculated into vertical displacement, then, due to the hydrodynamic problem under consideration, with an instantaneous piston movement, the ocean surface will rise by the same amount as the block at the bottom [26]. Depending on the speed of movement of the keyboard blocks in the seismic source, various scenarios for the formation of a tsunami source on the water surface can be realized. Using (2), the estimated displacements of the Earth's crust in the earthquake source were obtained (see Table 2).

Table 2. Characteristic parameters of the earthquake source and displacement of the Earth's crust in the source during the earthquake on October 30, 2020 in the Aegean Sea.

Parameter	Characteristic parameters of earthquake 10.30.2020
Magnitude of the earthquake	7
The length of the rupture plane (km)	34
Width of the rupture plane (km)	12
Water surface displacement (m)	1,2

So, for the earthquake under consideration at $M = 7$, the approximate values of the size of the earthquake source obtained by (1) and the maximum displacement height in the earthquake source of about 1.2 m found by (2) are used to simulate the generation of the tsunami source and further propagation of waves across the water area.

Figure 4 shows the water area under consideration with the marked epicenter of the earthquake and aftershocks of the first day of the earthquake, as well as with points located on the continental and island coasts of the water area, where tsunami waves were recorded.
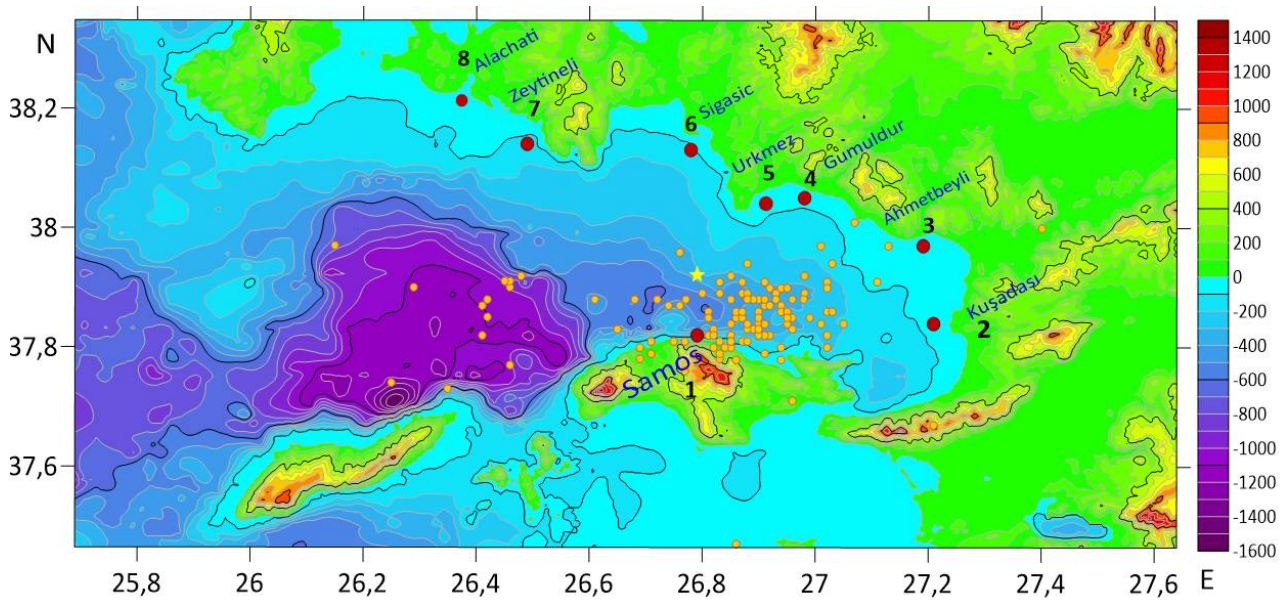
Fig. 4. The considered water area, the epicenter of the earthquake and aftershocks of the first day of the earthquake on October 30, 2020 in the Aegean Sea. The red dots mark the position of the virtual tide gauges.

3. MATHEMATICAL FORMULATION OF THE PROBLEM

To consider the process of generating tsunami waves in the keyboard model of a seismic source and their propagation over the water area, we will use the shallow water equations (see, e.g. [35]). The geometry of the problem is shown in Fig. 5. The schematic sketch at the bottom is presented in the form of a rectangular keyboard block, height $B(x, y, t)$ and transverse dimensions, limited by the vertical sides of the rectangle; α is the angle of inclination of the shelf to the horizon, L_{sh} is the shelf length [28-32].
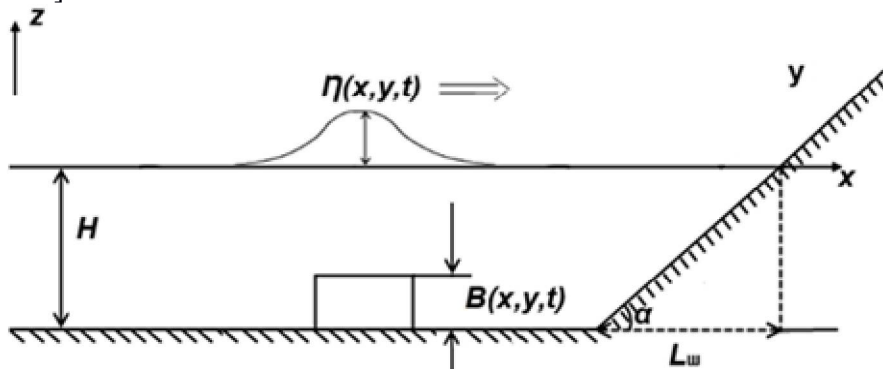

Fig. 5. Schematic representation of wave generation.

In 2D case, the system of nonlinear shallow water equations can be written as [35]

6

$$\begin{cases} \dfrac{\partial u}{\partial t} + u\dfrac{\partial u}{\partial x} + v\dfrac{\partial v}{\partial y} + g\dfrac{\partial \eta}{\partial x} = 0 \\[2mm] \dfrac{\partial v}{\partial t} + u\dfrac{\partial v}{\partial x} + v\dfrac{\partial v}{\partial y} + g\dfrac{\partial \eta}{\partial y} = 0 \\[2mm] \dfrac{\partial \eta}{\partial t} + \dfrac{\partial}{\partial x}[(\eta + H - B)u] + \dfrac{\partial}{\partial y}[(\eta + H - B)v] = \dfrac{\partial B}{\partial t} \end{cases} \qquad (3)$$

here $u\,(x, y, t)$, $v\,(x, y, t)$ are the velocity components, $h\,(x, y, t)$ is the disturbance of the free surface, $H\,(x, y)$ is the depth of the basin, $B\,(x, y , t)$ is the change in the bottom of the basin (taking into account the characteristics of the dynamic seismic source), g is the acceleration of gravity. In this work, $B(x, y, t)$ is the function describes the sequential movement of the keyboard blocks. The modeling of such a process in the earthquake source, which would most fully correspond to possible movements occurring in the vicinity of the earthquake source in the first minutes after the onset of the earthquake, is considered.

4. NUMERICAL SIMULATION

From the set of difference schemes approximating Eqs. (3), the numerical scheme of Sielecki and Wurtele was taken [34], modified for computation the generation of a long wave by a dynamic underwater source, which has a second order of approximation. The paper presents two possible scenarios for the realization of the movements of the Earth's crust in the seismic source during the earthquake of October 30, 2020 in the water area of the Aegean Sea.

SCENARIO 1

In Scenario 1, a virtual earthquake source is considered, segmented into 2 blocks, located along the island zone where the earthquake occurred. Based on the data obtained on the earthquake source size (Table 2), as well as the data on the localization of the epicenter of the earthquake and aftershocks [6] and also, taking into account the tectonic setting for this region, where active tension and shear deformations coexist [5], the bathymetry of the considered water area there were built two possible sources of the earthquake. Figure 6 shows a bathymetric map of the computed water area. The red line outlines the virtual seismic source of the earthquake, segmented into 2 blocks. The burgundy line marks the fault line during the earthquake of October 30, 2020 in the Aegean Sea. Blue dots mark points on the coast for which there is documentary data on the tsunami run-up.

Table 3 shows the characteristics for the kinematic motion of two blocks in the earthquake source. The movement begins with the first block, moving vertically upward for 15 s to a height of 1.2 m. 5 s after the beginning of the movement of the first block, the second block begins to move vertically downward at a distance of 1m, the movement occurs for 10 s, and ends simultaneously with the rise of the first block. Then, after 3 s, the same block is shifted upward to a height of 0.8 m. The total movement time of the blocks is 24 s [6].

Table 3. Characteristics of the kinematic movement of blocks for Scenario 1.

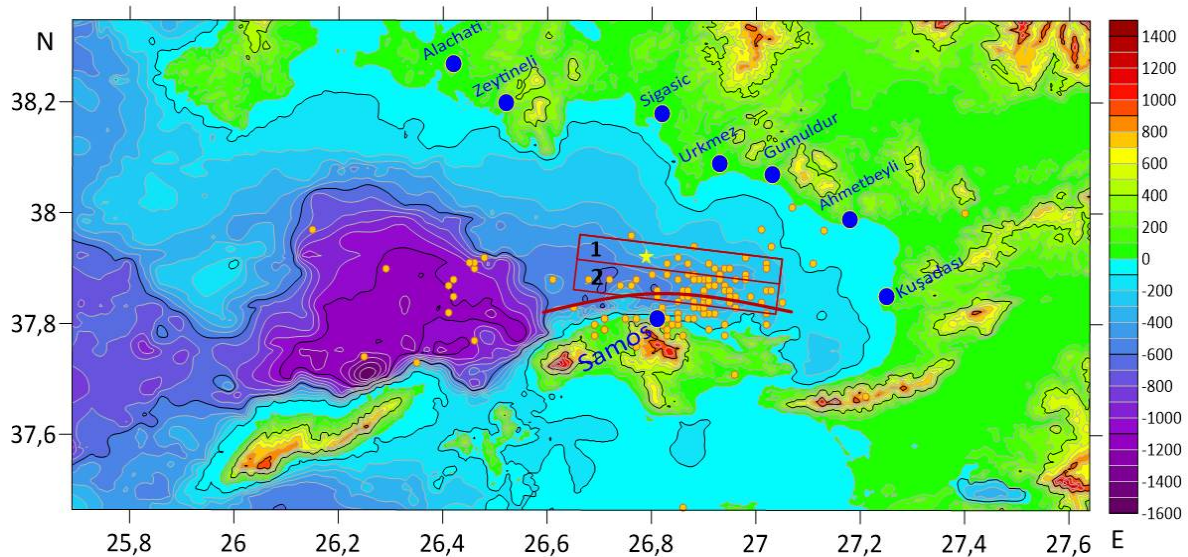| Block number	1	2	2
Start time (s)	0	5	18
Final time of movement (s)	15	10	6
Height of movement (m)	1,2	-1	0,8

Vol 40 No. 3, page 184 (2021)

Fig. 6. Schematic representation of a two-block earthquake source on October 30, 2020 in the Aegean Sea (Scenario 1). The bold red line is the fault line. Blue points indicate localization of 8 points under consideration on the coast.

Fig.7-9 show the simulation results for Scenario 1. Fig.7 shows the generation of the tsunami source. Since, due to the incompressibility of the liquid and the hydrostatic pressure, the ocean surface will rise by the same amount by which the block at the bottom has been displaced [26], then, according to the parameters of Table 3, panel 1 (Fig. 6) shows the displacement of the water surface when the first block rises. 5 s after the start of the movement, block 2 begins to move downward, which corresponds to the displacement of the wave surface above the second block (panel 2). The movement of block 2 ends in 10 s simultaneously with the stop of block 1. After a 3 s delay, block 2 begins to move upward, which leads to an upward shift (panel 4). Thus, the source of the tsunami, i.e. displacement of the wave surface, is formed in 24 s, after which the wave propagates over the sea area.
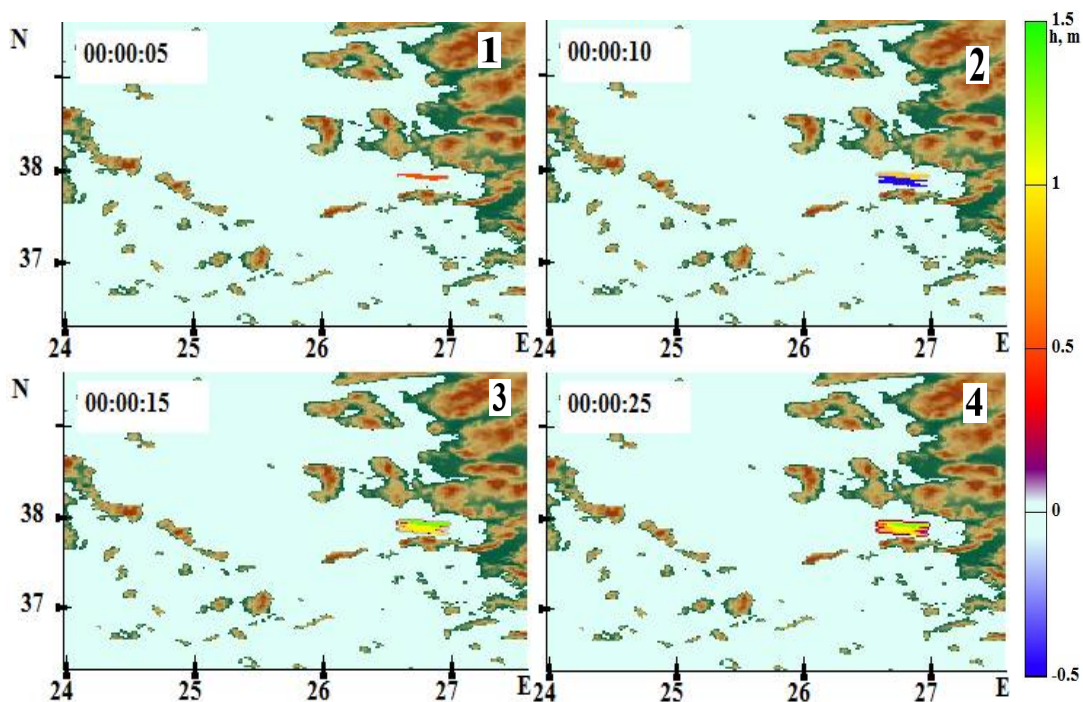

Fig. 7. Generation of a tsunami source during the implementation of Scenario 1 for four time points.

Vol 40 No. 3, page 185 (2021)

8

Figure 8 (panels 1-8) shows the position of the wave fronts. It is clearly seen that after about 2min 30s (panel 1) waves with a height of 1.25m reach the Samos Island.
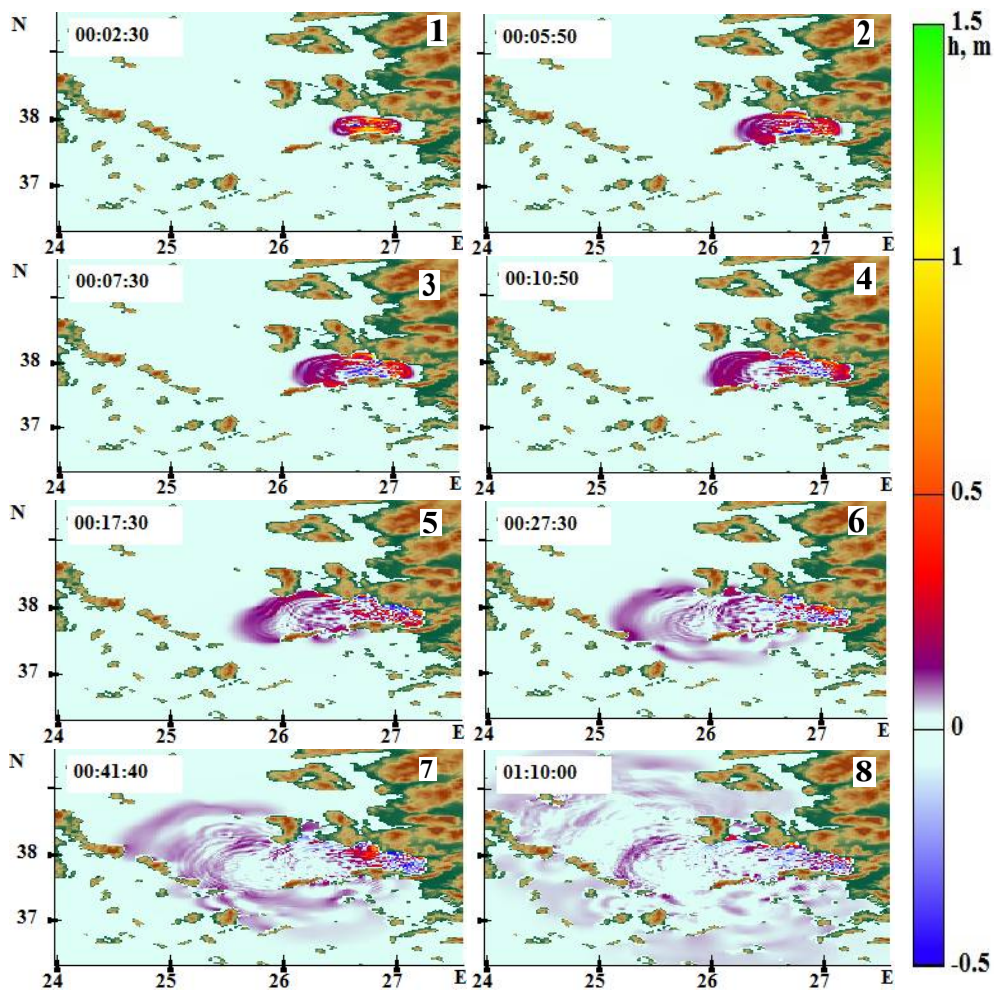

Fig.8. Propagation of wave fronts in the implementation of Scenario 1
for eight time points.

After 5min 50s (panel 2), the wavefront reached the coastal city of Urkmez. For 7 min 30 s (panel 3) a wave with a height of 1.06 m reached the city of Ahmetbeyli, and after about 10 min and 50 s, the front reached the largest city on the coast - Kusadasi 1.2 m (panel 4). At 17.5 min, we see a height of about 1.31m in the area of the city of Zeytineli (panel 5). In 27.5 min in the coastal town of Alacati, the height reached 0.92 m (panel 6).
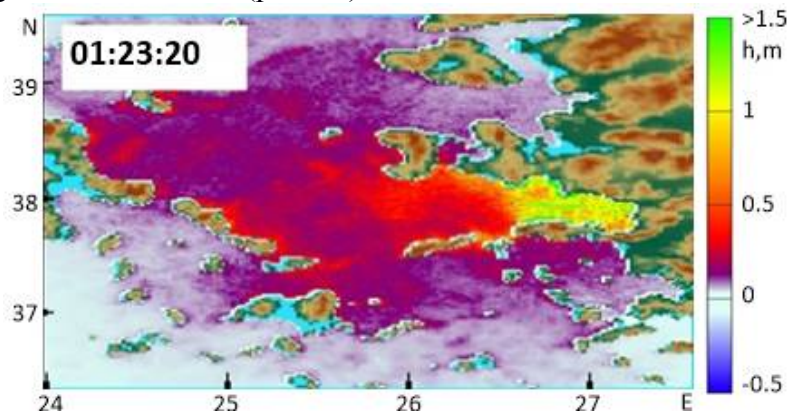

Fig. 9. Distribution of maximum wave heights over the water area during
the implementation of Scenario 1.

Figure 9 shows the distribution of the maximum wave heights over the entire computed area. The distribution of the maximum wave heights clearly shows that the most dangerous areas are near-field points, namely the island, the cities of Izmir and Kusadasi. Fig.10 shows a 3D histogram of the distribution of the maximum heights of tsunami waves along the coasts of the computed water area. It can be seen that the maximum wave height in the area of Kusadasi does not exceed 0.6 m. On the island of Samos, heights vary from 0.6 to 1.7 m from west to east. On the coast of the city of Urkmez, the maximum wave height reached 1.3 m, but decreases towards the Pamudjak beach to 0.5 m.
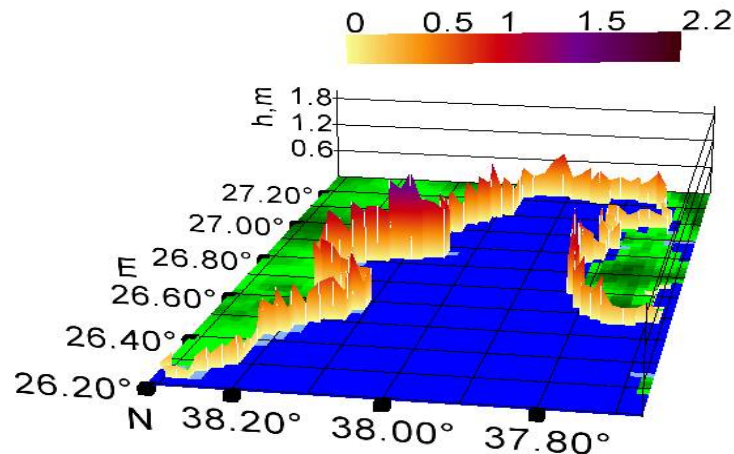

Fig. 10. 3D histogram for a two-block source in the implementation of Scenario 1.

It should be noted that the observed maximum wave heights near the coast, which are closer to the source, are many times higher than those located at more distant points from the earthquake source.

SCENARIO 2

In Scenario 2, a virtual earthquake source is considered, segmented into 3 blocks, located along the fault zone where the earthquake occurred. It can be seen that the arrangement of the blocks follows the line of the oblique subduction zone (Fig. 11). Table 4 shows the characteristics for the motion of three blocks in the earthquake source. The movement begins with the second block, moving vertically upward for 15 s to a height of 1.2 m in 15 s. 5 s after the start of the movement of the first block, the third block begins to move upward at a distance of 1 m in 15 s. 5 s after that, the third block begins its downward movement by 0.8 m in 14 s. The total movement time of the blocks is 24 s [6].

Table 4. Characteristics of the kinematic movement of blocks for Scenario 2.

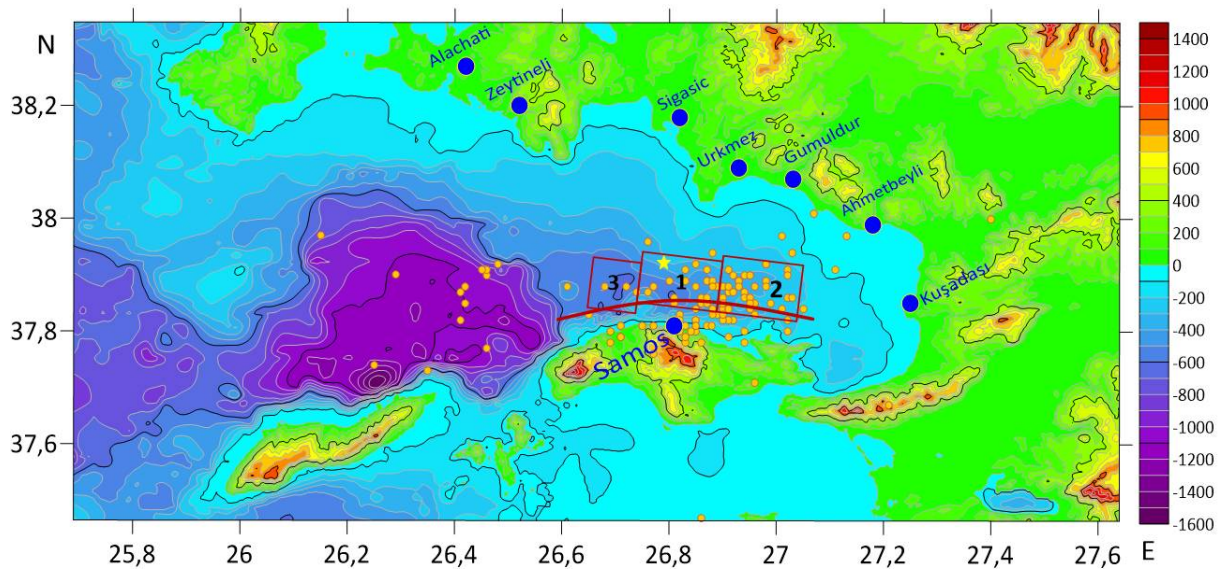| Block number	2	3	1
Start time (s)	0	5	10
Final time of movement (s)	15	15	14
Height of movement (m)	1,2	1	-0,8

Fig. 11. Schematic representation of the three-block source of the earthquake on October 30, 2020 in the Aegean Sea. The bold red line is the fault line. Blue points indicate localization of 8 points under consideration on the coast.

The computation results for a three-block source are shown in Figures 11-13. In Fig. 12 it can be seen that, according to the dynamics of the movement of blocks in the earthquake source: first, block 2 moves up, then, 5 s after the beginning of the movement of the first block, block 3 begins to move and then, block 1 moves down (Table 4), occurs displacement of the water surface above the blocks and the formation of a tsunami source.
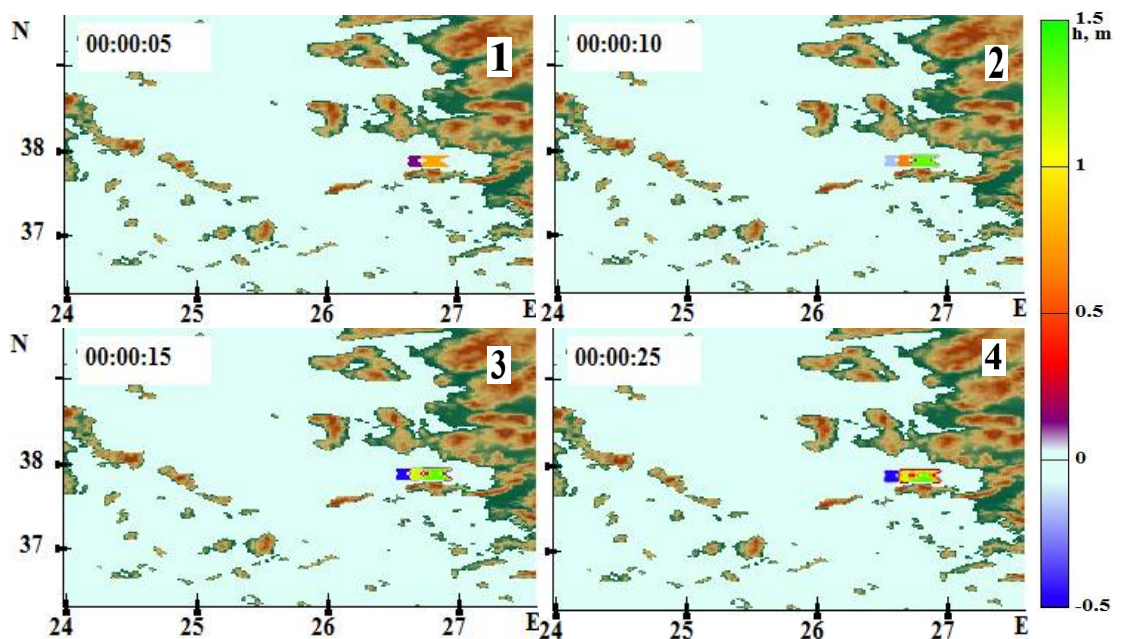

Fig. 12. Generation of the tsunami source in the implementation of Scenario 2 for 4 time points.

Figure 13 shows the propagation of wave fronts in the implementation of this scenario over the computed water area.
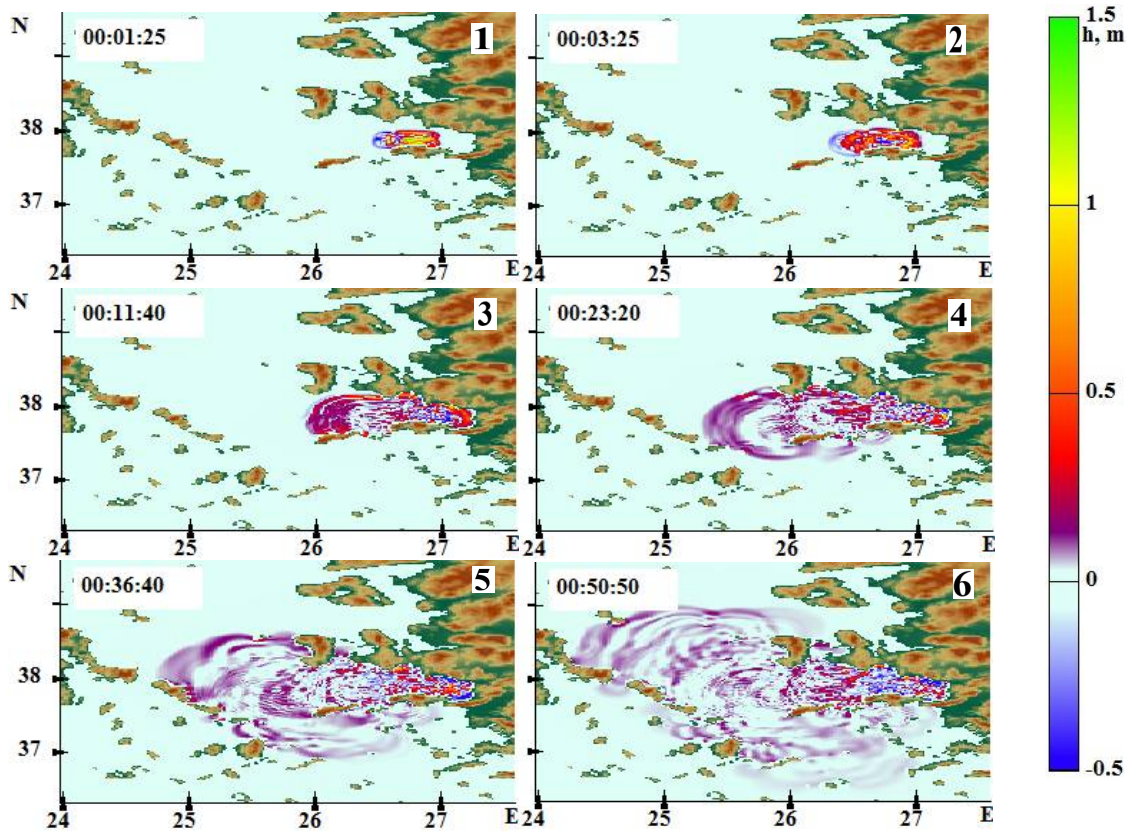
Fig. 13. Propagation of wave fronts in the implementation of Scenario 2 for 6 time moments.

It is clearly seen that after about 1 min 25 s (panel 1) waves with a height of 1.31 m reach the Samos Island. After 3 min 25 s (panel 2), the wave front reached the coastal town of Urkmez 1.65 m. At 11:40 a.m. (panel 3) a wave with a height of 1.26 m reached the city of Ahmetbeyli, and after about 23:20 min the front reached the largest city on the coast - Kusadasi 1.14m (panel 4). At 36:40, a height of about 1.0 m is seen in the area of the city of Zeytineli (panel 5). At 55:50 the wave reached the entire coastline, in the coastal town of Alacati the height reached 0.6 m (panel 6).

Figure 14 shows the 3D distribution of the maximum wave heights along the coasts of the considered water area. It can be seen that the most dangerous areas are near-field points, namely the island of Samos, the cities of Izmir and Kusadasi. The maximum wave height in the area of Kusadasi does not exceed 0.5 m. On the island of Samos, heights vary from 0.5 to 1.8 m from west to east. On the coast of the city of Urkmez, the maximum wave height reached 1.03 m, but decreases towards the Pamudjak beach to 0.36 meters. The observed maximum wave heights near the coast, which are closer to the source, are many times higher than those located at more distant points from the source of the earthquake.
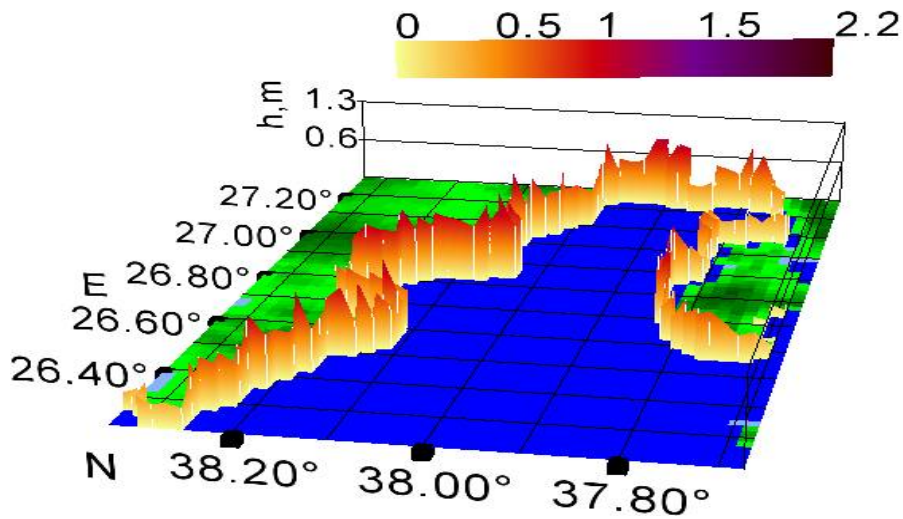
12

Fig. 14. 3D histogram for a three-block source in the implementation of Scenario 2.

Fig. 15 shows data from virtual tide gauges when computed according to Scenario 2. It is clearly seen that the first displacement on tide gauges corresponds to the character of the tsunami wave run up to this point (see, for example, [5,6]).
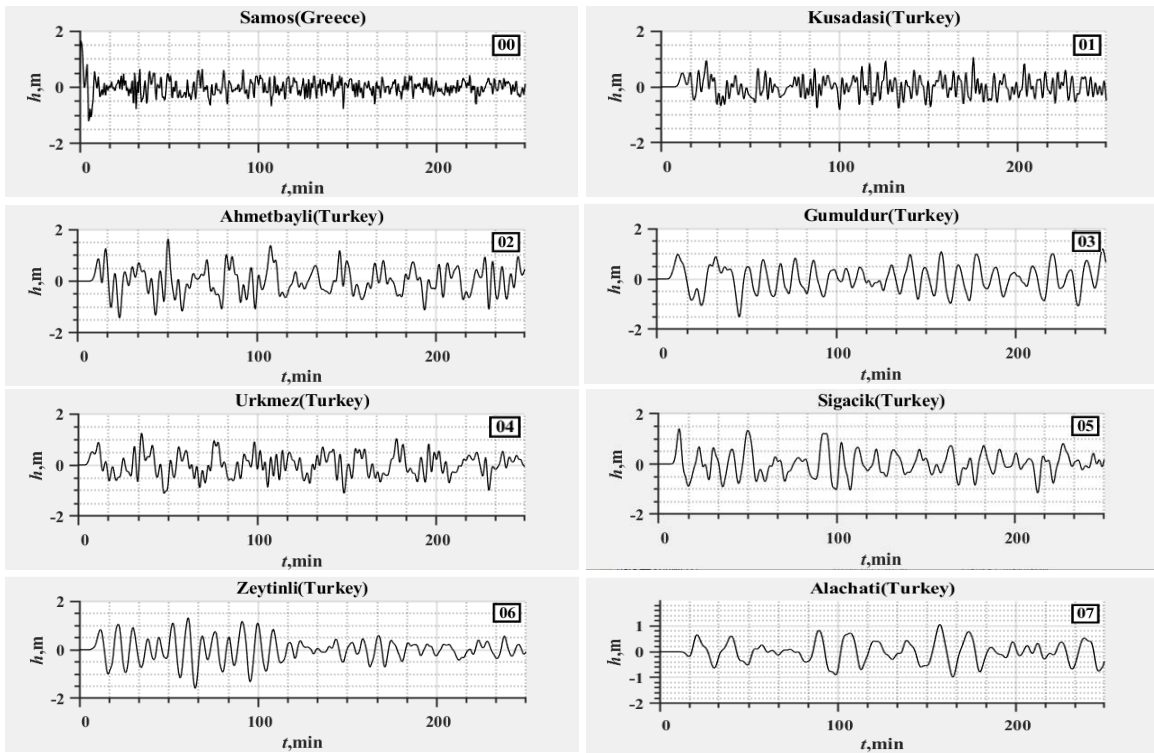

Fig. 15. The virtual tide-gauge records for points 1-8 (Scenario 2).

5. COMPARISON OF COMPUTATION RESULTS WITH REAL DATA AND DATA OF OTHER AUTHORS

Table 5 shows a comparison of computed data with real ones taken from work [6]. It is clearly seen that the results of the first computation (Scenario 1) for a two-block source are rather far from real data. Taking into account the presence of an oblique subduction zone (see Fig. 5, red fault line), the earthquake source was considered in more detail describing this fault zone (see Fig. 10). Using the available characteristics of the earthquake and manifestations of tsunami waves at specific points on the coast (see, for example, [6]), a number of scenarios for the kinematic movement of blocks in the earthquake source of this form were considered, one of which is given in this work (Scenario 2). The results of numerical simulations for Scenario 2 show a closer agreement with field data than for Scenario 1. Some difference between arrival times observed is due to problem with location of real and virtual tide gauges in computations and real event. Moreover, the arrival time in several points was estimated during post-event field survey only from eyewitness accounts and photos.

Table 5. Comparison of computation results with documentary data.

Point	Real data on wave height on the beach, м	Wave height at 3m isobate (Scenario 1), м	Wave height at 3m isobate (Scenario 2), м
1.Samos (Greece)	1.8 [24]	1.23	1.65
2.Kusadasi (Turkey)	1.5 [6]	1.05	1.06
3.Ahmetbayli(Turkey)	1.34 [6]	1.04	1.64
4.Gumuldur (Turkey)	1.86 [6]	1.14	1.20
5.Urkmez (Turkey)	1.68 [6]	1.16	1.24
6. Sigacik (Turkey)	1.5 [6]	1.44	1.40
7.Zeytinli (Turkey)	1.5 [6]	1.24	1.31
8. Alachati (Turkey)	1.00 [6]	0.60	1.05
9.Bodrum (Turkey)	0.04 [5]	0.048	0.061
10.Kos (Greece)	0.10 [5]	0.042	0.061
11.Syros (Greece)	0.080 [5]	0.066	0.083
12.Plomari (Greece)	0.05 [5]	0.082	0.075

The distribution of the maximum wave heights over the computation water area is clearly seen in Figures 16 and 17, which show the data of numerical simulation according to scenario 2 and data from [6]. It can be seen that the distribution pattern along the coastal zone is fairly close.
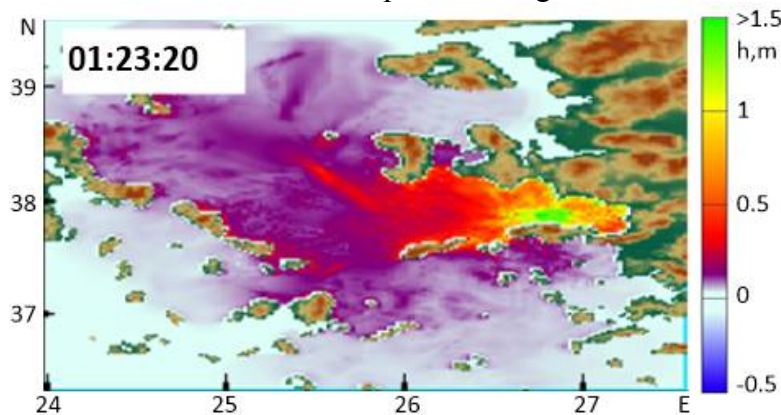

Fig. 16. Distribution of maximum water surface elevations in Eastern Aegean computed in the far-field simulations within the keyboard model of the earthquake source.
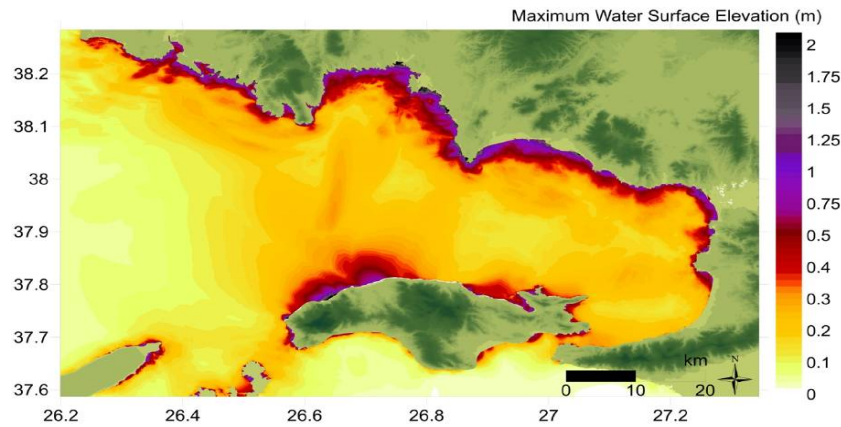
Vol 40 No. 3, page 191 (2021)

Fig. 17. Distribution of maximum water surface elevations in Eastern Aegean computed in the far-field simulations via NAMI DANCE [6].

6. CONCLUSIONS

The paper considers one of the strong tsunamigenic earthquakes that occurred in the Aegean Sea in the 21st century. Using the keyboard model of the earthquake source, two variants of seismic sources were considered: two-block and three-block sources, localized along the fault zone. Based on the data of available tide gauge records [5] and works on the analysis of tsunami wave manifestations on a number of coasts of the Aegean Sea [1], a dynamic process in the earthquake source generating tsunami waves was numerically simulated. The closest results were obtained when considering the generation of a tsunami by a three-block source (Scenario 2). The computations were carried out up to the 3-meter isobath, which is associated with complex coastal bathymetry and which made it possible to reduce the computation time. Since the goal of numerical modeling is to obtain an adequate distribution of the maximum wave heights along the considered coasts, it can be seen that the data obtained agree with this process well. It should be noted that when modeling according to Scenario 2, for a number of points under consideration, where tide gauge data were absent, but coastal survey data are well represented, the results obtained showed somewhat underestimated values. However, taking into account that, when recalculated from the isobath to the dry coast, the height of the maximum tsunami run-up may increase (see, for example, [36,37], it can be concluded that the numerical simulation data are in good agreement with the documented data (see Table 5).

REFERENCES

1. http://www.ioc-sealevelmonitoring.org/ Tsunami Bulletin Board, Tsunami Information Center (ITIC)

2. http://www.en.unesco.org

3. http://www.gdacs.org

4. https://accelnet.gein.noa.gr/2020/11/09/the☐earthquake☐of☐october☐30th☐2020☐atsamos☐ eastern☐aegean☐sea☐greece☐preliminary☐report/

5. Dogan G.G., A.C.Yalciner, Y.Yuksel, E.Ulutaş, O.Polat, I.Güler, C.Şahin, A.Tarih, U.Kânoğlu *The 30 October 2020 Aegean Sea Tsunami: Post-Event Field Survey Along Turkish Coast //* Pure Appl Geophys 178, No.3, 785–812 (2021);

6. Cetin, K.O.; Mylonakis, G.; Sextos, A.; Stewart, J.P. Seismological and Engineering Effects of the M 7.0 Samos Island (Aegean Sea) Earthquake; Report GEER-069; Geotechnical Extreme Events Reconnaissance Association: Alameda County, CA, USA, 2021.

7. Altınok, Y., Alpar, B., Ozer, N., & Vardar, H. (2011). Revision of the tsunami catalogue affecting Turkish coasts and surrounding regions. Natural Hazards and Earth System Sciences, 11(2), 273–291.

8. Altınok, Y., & Ersoy, S. (2000). Tsunamis observed on and near the Turkish coast. Natural Hazards, 21, 185–205

9. Ambraseys, N. N. (1962). Data for the investigation of the seismic sea-waves in the Eastern Mediterranean. Bulletin of the Seismological Society of America, 52(4), 895–913.

10. Ambraseys, N., & Synolakis, C. (2010). Tsunami catalogs for the Eastern Mediterranean, revisited. Journal of Earthquake Engineering, 14(3), 309–330.

11. Kuran, U., & Yalciner, A. C. (1993). Crack propagations, earthquakes and tsunamis in the vicinity of Anatolia. In S. Tinti (Ed.), Tsunamis in the world. Advances in natural and technological hazards research (Vol. 1, pp. 159–175). Springer. https://doi.org/ 10.1007/978-94-017-3620-6_13

12. Minoura, K., Imamura, F., Kuran, U., Nakamura, T., Papadopoulos, G. A., Takahashi, T., & Yalciner, A. C. (2000). Discovery of Minoan tsunami deposits. Geology, 28(1), 59–62.

13. Papadopoulos, G. A., & Chalkis, B. J. (1984). Tsunamis observed in Greece and the surrounding area from antiquity up to the present times. Marine Geology, 56(1–4), 309–317.

14. Papadopoulos, G. A., Gra`cia, E., Urgeles, R., Sallares, V., De Martini, P. M., Pantosti, D., et al. (2014). Historical and prehistoric tsunamis in the Mediterranean and its connected seas: geological signatures, generation mechanisms and coastal impacts. Marine Geology, 354, 81–109.

15. Tinti, S., Maramai, A., & Graziani, L. (2001). A new version of the European tsunami catalogue: updating and revision. Natural Hazards and Earth System Sciences, 1, 255–262.

16. Beisel, S., Chubarov, L., Didenkulova, I., Kit, E., Levin, A., Pelinovsky, E., et al. (2009). The 1956 Greek tsunami recorded at Yafo, Israel, and its numerical modeling. Journal of Geophysical Research Oceans, 114, C09002. https://doi.org/10.1029/ 2008JC005262

17. Okal E.A., Synolakis C.E., Uslu B., Kalligeris N., & Voukouvalas E. (2009). The 1956 earthquake and tsunami inAmorgos, Greece. Geophysical Journal International, 178(3), 1533–1554.

18. Papadopoulos, G. A., & Pavlides, S. B. (1992). The large 1956 earthquake in the South Aegean: macroseismic field configuration, faulting, and neotectonics of Amorgos Island. Earth and Planetary Science Letters, 113(3), 383–396.

19. Papazachos, B. C., Koutitas, C., Hatzidimitriou, P. M., Karacostas, B. G., & Papaioannou, C. A. (1985). Source and short-distance propagation of the July 9, 1956 southern Aegean tsunami. Marine Geology, 65(3–4), 343–351.

20. Yalciner, A. C., Kuran, U., Akyarli, A., & Imamura, F. (1995). An investigation on the propagation of tsunamis in the Aegean Sea by mathematical modeling. In Y. Tsuchiya & N. Shuto (Eds.), Tsunami: progress in prediction, disaster prevention and warning. Advances in natural and technological hazards research (Vol. 4, pp. 55–70). Springer. https://doi.org/10.1007/978-94-015-8565-1_4

21. Kalogeras I., N.S. Melis, N. Kalligeris, *The earthquake of October 30th, 2020 at Samos, Eastern Aegean Sea, Greece,* https://accelnet.gein.noa.gr/_Reports/Samos_ Preliminary_ Report_EN.pdf (last access 16/2/2021).

22. Triantafyllou, I, Gogou, M, Mavroulis, S, Katsetsiadou, KN, Lekkas, E, and Papadopoulos, G, 2020. The tsunami caused by the 30 October 2020 Samos (Greece), East Aegean Sea, Mw6.9 earthquake: impact assessment from post□event field survey and video records. Report published at EMSC: https://edcm.edu.gr/images/docs/2020/Samos2020□TSUNAMI□REP/ pdf

23. Tani O., E.E. Papadimitrious, Z. Pabuccu, V.Karakostas, A.Yoruk, and K.Leptokaropoulos A *Detailed Analysis of Microseismicity in Samos and Kusadasi (Eastern Aegean Sea) Areas* // Acta Geophysica (2014) 62(6), 1283-1309. DOI: 10.2478/s11600-013-0194-1.

24. Triantafyllou I., M.Gogou, S.Mavroulis, E.Lekkas, G.A.Papadopoulos, M.Thravalos *The Tsunami Caused by the 30 October 2020 Samos (Aegean Sea)Mw7.0 Earthquake: Hydrodynamic Features, Source Properties and Impact Assessment from Post-Event Field Survey and Video Records* // J. Mar. Sci. Eng. (2021), 9, 68. https://doi.org/10.3390/jmse 9010068

25. Garagash I.A., L.I. Lobkovski, (2006). *An analysis of the dynamic displacement process of the sea bottom due to a subduction zone earthquake*. In: Proc. of 4th International FLAC Symposium on Numerical Modeling in Geomechanics (eds. Hart & Varona). Paper: 06-01 © 2006 Itasca Consulting Group, Inc., Minneapolis, ISBN 0-9767577-0-2

26. Pelinovsky, E.N. Hydrodynamics of Tsunami Waves (1996) // IAP RAS, Nizhny Novgorod, Russia.

27. Lobkovsky L.I., Baranov B.V. Keyboard model of strong earthquakes in island arcs and active continental margins, (1984) // Doklady. V.75. No. 4. S. 843-847.

28. Lobkovsky L.I., R.Mazova, Baranov B.V., Kataeva L.U. (2006), Generation and propagation of tsunamis in the Sea of Okhotsk: possible scenarios // Doklady, pp.528-532.

29. Lobkovsky L.I., R.Mazova, Baranov B.V., Kataeva L.U. (2006). Tsunami modeling in the Sea of Okhotsk based on the keyboard model of the subduction zone // in the book: Fundamental research of the oceans and seas (edited by N. Laverov), Moscow: Nauka, book 1, p. 292-303.

30. Lobkovsky L.I., Mazova R.Kh., Kolchina E.A. (2014) *Estimation of Maximum Heights of Tsunami Waves for the Sochi Coast from Strong Submarine Earthquakes*, Doklady. Earth Sciences V.456, PP. 749–754. DOI:10.1134/S1028334X14060269

31. Lobkovsky L., R.Mazova, S.Tyuntyaev, I.Remizov, (2016). *Features and Problems with Historical Great Earthquakes and Tsunamis in the Mediterranean Sea* // Journal Science of Tsunami Hazards, Vol. 35, .No. 3, pp. 167 – 188.

32. Mazova R.Kh., Moiseenko T., Kurkin A.A., Jorge Van Den Bosch F., Gustavo Oses A. (2021). *Numerical Simulation of a Catastrophic Earthquake and Strong Tsunami of April 1, 2014 near the Northwestern Part of the Chilian Coast.* Journal Science of Tsunami Hazards V.40,N.2,pp.83-100.

33. Wells D.L., Coppersmith K.J. (1994), *New empirical relationships among magnitude, rupture length, rupture width, rupture area, and surface displacemen*t // Bull. Seism. Soc. Am. Vol. 84. P. 974-1002 .

Vol 40 No. 3, page 194 (2021)

34. Sielecki A., Wurtele M. (1970), *The numerical integration of the non-linear shallow-water equations with sloping boundaries* // J. Comp. Phys. V.6, P.219-236.

35. Voltzinger N.E., Klevanny K.A., Pelinovsky, E.N. Long-wave dynamics of the coastal zone, Leningrad: Gidrometeoizdat, 1989.- 272 p

36. Mazova, R.Kh. (1984). *On the approximate boundary conditions at the shoreline, convenient for the numerical calculation of the run-up of tsunami waves* // in the book: Generation of tsunami waves and the emergence of waves on the coast, (Radio and Communication Press, Moscow, USSR), 54-57.

37. Pelinovsky E.N., Mazova R.Kh. *Exact analytical solutions of nonlinear problems of tsunami wave runup on slopes with different profiles* // Natural Hazards V.6, P.227-241, 1992.

20. Dogan, G. G., Annunziato, A., Papadopoulos, G. A., Guler, H. G., Yalciner, A. C., Cakir, T. E., et al. (2019). The 20th July 2017 Bodrum-Kos Tsunami field survey. Pure and Applied Geophysics, 176, 2925–2949. https://doi.org/10.1007/s00024-019-02151.

37. Papadopoulos, G.A.; Gràcia, E.; Urgeles, R.; Sallares, V.; De Martini, P.M.; Pantosti, D.; González, M.; Yalciner, A.C.; Mascle, J.; Sakellariou, D.; et al. (2014), Historical and pre-historical tsunamis in the Mediterranean and its connected seas: Geological signatures, generation mechanisms and coastal impacts. Mar. Geol., 354, 81–109.

38. Heidarzadeh, M.; Necmioglu, O.; Ishibe, T.; Yalciner, A.C. Bodrum–Kos (Turkey-Greece) (2017), Mw6.6 earthquake and tsunami of 20 July 2017: A test for the Mediterranean tsunami warning system. Geosci. Lett., 4, 31.

39. Cankaya ZC, Suzen ML, Yalciner AC, Kolat C, Zaytsev A, and Aytore B.(2016), A new GIS-based tsunami risk evaluation: MeTHuVA (METU tsunami human vulnerability assessment) at Yenikapı, Istanbul. Earth, Planets and Space, 68(1), 133.

40. England, P, Howell, A, Jackson, J, and Synolakis C, (2015), Palaeotsunamis and tsunami hazards in the Eastern Mediterranean. Philosophical Transactions of the Royal Society A: Mathematical, Physical and Engineering Sciences, 373(2053), p. 20140374.

41. Okal, EA, Synolakis, CE, Uslu, B, Kalligeris, N, and Voukouvalas, E, (2009), The 1956 earthquake and tsunami in Amorgos, Greece. Geophysical Journal International, 178(3), 1533-1554.

42. UNESCO, 2014. International Tsunami Survey Team (ITST) Post☐Tsunami Survey Field Guide. 2nd Edition. IOC Manuals and Guides No.37, Paris: UNESCO 2014 (English).

44. Yalciner, AC, Imamura, F, and Synolakis C. (2008). *Amplitude evolution and eunup of long waves; Comparison of experimental and numerical data on a 3D complex topography*. In Advanced Numerical Models for Simulating Tsunami Waves and Runup (ed. by: Philip L-F Liu, H.Yeh, C.Synolakis): Advances in Coastal and Ocean Engineering: V10, pp.243-247. https://doi.org/10.1142/6226.

45. Soloviev S.L., Gu Ch.N., Kim Kh.S., Solovieva O.N., Shchetnikov N.A. Tsunami in the Mediterranean. 2000 BC - 1991 (Moscow: Scientific world, 1997).

Á